Available online at www.sciencedirect.com
ScienceDirect
Journal of Power Sources 159 (2006) 468–477
JOURNAL OF POWER SOURCES
www.elsevier.com/locate/jpowsour

Humidity of reactant fuel on the cell performance of PEM fuel cell with baffle-blocked flow field designs

Jer-Huan Jang [a], Wei-Mon Yan [b,*], Hung-Yi Li [b], Yeh-Chi Chou [b]

[a] *Department of Mechanical Engineering, Northern Taiwan Institute of Science and Technology, Beitou, Taipei 112, Taiwan, ROC*
[b] *Department of Mechatronic Engineering, Huafan University Shih Ting, Taipei 22305, Taiwan, ROC*

Received 14 June 2005; received in revised form 28 June 2005; accepted 11 July 2005
Available online 18 January 2006

Abstract

The objective of this work is to examine the effects of humidity of reactant fuel at the inlet on the detailed gas transport and cell performance of the PEM fuel cell with baffle-blocked flow field designs. It is expected that, due to the water management problem, the effects of inlet humidity of reactant fuel gases on both anode and cathode sides on the cell performance are considerable. In addition, the effects of baffle numbers on the detailed transport phenomena of the PEM fuel cell with baffle-blocked flow field are examined. Due to the blockage effects in the presence of the baffles, more fuel gas in the flow channel can be forced into the gas diffuser layer (GDL) and catalyst layer (CL) to enhance the chemical reactions and then augment the performance of the PEMFC systems. Effect of liquid water formation on the reactant gas transport is taken into account in the numerical modeling. Predictions show that the local transport of the reactant gas, the local current density generation and the cell performance can be enhanced by the presence of the baffles. Physical interpretation for the difference in the inlet relative humidity (RH) effects at high and low operating voltages is presented. Results reveal that, at low voltage conditions, the liquid water effect is especially significant and should be considered in the modeling. The cell performance can be enhanced at a higher inlet relative humidity, by which the occurrence of the mass transport loss can be delayed with the limiting current density raised considerably.

Keywords: Modeling; Flow field design; PEM fuel cell

1. Introduction

It has been a period of time that the attention on the modeling of fuel cell has been drawn since the early 1990s. One of the most promising types of fuel cells, the proton exchange membrane fuel cell (PEMFC), is currently being aggressively researched due to its significant advantages in portable electronic applications over conventional battery systems. It also meets more stringent emissions standards because far fewer pollutants produced than that of internal combustion engines. In previous studies, many pioneers have contributed to the modeling of fuel cells. Most early studying is one-dimensional (ID) or two-dimensional (2D) flows [1–4]. Bernadi and Verbruge [1] developed a ID hydraulic model assuming that the membrane is fully saturated with water and that most of the water is transported through the electrodes in the liquid phase. Springer et al. [2] proposed an isothermal, one-dimensional model for the proton exchange membrane fuel cells. In their model, water diffusion coefficient, electro-osmotic drag coefficient, water sorption isotherms and the membrane conductivities were assumed to be functions of membrane water content. The first quasi-2D, along-the-channel model of a PEM fuel cell was established by Fuller and Newman [3] with the assumption of constant diffusivity of water in membrane to study water and thermal management issues. Nguyen and White [4] proposed a model of the water and heat management of the PEMFC systems, which includes the effect of electro-osmosis, diffusion of water, heat transfer from solid phase to gas phase and latent heat as water evaporation and condensation.

The stability of the membrane is determined by its water content. Proper hydration of the membrane is critical for maintaining membrane conductivity and mechanical stability [5,6]. Various humidification designs such as internal humidification, external humidification and direct injection methods are used in the

* Corresponding author. Tel.: +886 2 26632102; fax: +886 2 26632143.
E-mail address: wmyan@huafan.hfu.edu.tw (W.-M. Yan).

0378-7753/$ – see front matter © 2005 Elsevier B.V. All rights reserved.
doi:10.1016/j.jpowsour.2005.07.096

Nomenclature

a	chemical activity of water vapor in cathode
Aj_0	reference exchange current density ($A\,m^{-2}$)
C_F	quadratic drag factor
C	concentration
D	diffusivity ($m^2\,s^{-1}$)
i	current density due to potential difference ($A\,m^{-2}$)
j	current density due to chemical reaction ($A\,m^{-3}$)
k	permeability (m^2)
M	molecular weight
P	pressure (atm)
P	partial pressure for i species (atm)
R	universal gas constant ($8.314\,mol^{-1}\,K^{-1}$)
s	the ratio of the volume of pore occupied by liquid water to the volume of pore in the porous medium
S	source term in momentum equation
S_c	source term of chemical reaction in the species concentration equation
S_j	source term in phase potential equation
S_L	source term with consideration of liquid water in the species concentration equation
T	temperature (K)
U, V	velocities in the X- and Y-direction ($m\,s^{-1}$)
X, Y	rectangular coordinate system (m)
Z	number of electrons transferred
Z_f	charge transfer coefficient

Greek letters

α	charge transfer rate
ε	porosity
η	overpotential
ν	kinematic viscosity ($m^2\,s^{-1}$)
Φ	membrane potential
ρ	density ($kg\,m^{-3}$)
σ	electric conductivity ($Q^{-1}\,m^{-1}$)
τ	tortuosity of the pore in the porous medium

Superscripts and subscripts

a	quantity in anode
c	quantity in cathode
eff	effective value
g	of gas diffuser layer
H^+	for proton
H_2	for hydrogen
H_2O	for water
I	for i species
m	of membrane
O_2	for oxygen
ref	reference value
sat	saturation pressure for water vapor
total	for total value
x	in the X-direction
y	in the Y-direction

PEMFC to maintain hydration level of the polymer membrane. Therefore, humidities of fuel and oxidant gases influence on the cell voltage performance and stability [7]. There are studies examined various aspects of PEMFC performance as a function of humidity [8,9]. However, the humidity is applied with external humidifiers. Water management is another important issue in the study of fuel cell. Yi and Nguyen [10] developed an along-the-channel model for evaluating the effects of various design and operating parameters on the performance of PEMFCs. They discovered that humidification of the anode gas is required to enhance the conductivity of the membrane, and the liquid injection and higher humidification temperature can improve the cell performance by introducing more water into the anode. Also applying a higher cathode gas pressure helps to replenish the water loss by electro-osmosis, thereby making the membrane more conductive and thus resulting in higher cell performance. A two-dimensional model was developed by Ge and Yi [11] to investigate the effects of operation conditions and membrane thickness on the water transport. In their study, the liquid water effect on the effective porosity for gas transport was considered to simplify the model of the two-phase flows in porous layers. The results revealed that the cell performance can be enhanced by increasing the cell temperature. However, the cell performance could not be obtained for higher humidity or saturation conditions. Baschuk and Li [12] established a mathematical model with variable degrees of water flooding in the PEMFC. Physical and electrochemical processes occurring in the membrane electrolyte, the cathode catalyst layer (CL), the electrode backing layer and the flow channel were considered. Compared with experimental results, they found that when air was used as the cathode fuel, the flooding phenomena are similar at different operating conditions of the pressures and temperatures. When cell pressure is increased significantly, the water flooding in the electrode becomes serious and leads to a noticeable reduction in the power output. Hsing and Futerko [13] developed a 2D model coupling fluid flow, mass transport and electrochemistry of a PEMFC taking into account the dependence of diffusion coefficient of liquid water in membrane. They found that the molar fractions of water are higher at the exit of flow channel. Furthermore, the molar fractions of water on the interface of flow channel and gas diffusion layer (GDL) decrease as the flow rate of hydrogen gas increases.

Designing flow field in bipolar plates of PEMFCs is one of the crucial factors to the cell performance. In order to augment the liquid water transport out of the GDL, a new flow channel design was developed by Nguyen [14]. This design works by converting the transport of reactant/product gases to/from the CL from diffusion mechanism to a convection mechanism. Um and Wang [15,16] constructed a multidimensional model to investigate the electrochemical kinetics, current distribution, fuel and oxidant flow and multicomponent transport in a PEMFC with the interdigitated flow field. He et al. [17] studied the effects of electrode and flow field design on the performance of a PEMFC with a half-cell model. It was found that the electrode performance would be increased with higher differential pressure between inlet and outlet channels. Increasing the electrode thickness is equivalent to increasing the diameter of a pipe in a fluid flow

system and the gas bypass effect becomes more significant. A 2D, steady half-cell model is constructed by Kazim et al. [18] to investigate the superiority of the interdigitated flow field design over the conventional one, especially in terms of maximum power density. The theoretical results show that the limiting current density of a fuel cell with an interdigitated flow field is about three times the current density of a fuel cell with a conventional flow field. The results also demonstrate that the interdigitated flow field design can double the maximum power density of a PEM fuel cell. Recently, Yan and co-workers [19,20] presented the studies about the effects of flow channel designs on the steady or dynamic gas transport and cell performance of PEM fuel cells. They found that the flow distributor geometry has a significant influence on the cell performance. They also discovered that the reactant transport and cell performance both can be enhanced by the presence of the baffles in the flow channel of the bipolar plate, especially at low voltage conditions. The beneficial baffle effects become increasingly remarkable with increasing width and/or number of baffles in the tandem array.

From the literatures reviews cited above, the optimal cell performance can be achieved with proper water management. The inlet relative humidity of reactant gases can lead to a result of a respective membrane dryness or membrane and electrode flooding. Therefore, it is essential to quantify the influence of relative humidities of reactant gases on the cell performance and transport phenomenon. It is also found that the efficiency of the thermal and water management in PEMFC systems can be enhanced with the appropriate design of the flow channel of the bipolar plate, especially with the interdigitated flow channel. However, the studies of fuel cells with interdigitated flow channel used the model with half-cell at cathode. This motivates the present study. The goal of this paper is to investigate the influence of inlet relative humidity of reactant gases on both anode and cathode on the cell performance and transport phenomenon with baffle-blocked flow field designs. A 2D numerical model of PEMFC with baffle-blocked in cathode flow channel design is developed to perform the exploration of the resultant transport phenomena and cell performance.

2. Analysis

In this study, a two-dimensional full cell model of the PEMFC with interdigitated flow channel is considered. The fuel cell with coordinate system is schematically illustrated in Fig. 1. The U and V are the velocity components in the X- and Y-directions, respectively. A parameter N is defined as the number of baffles inside the channels to study the baffle-block effect on the gas transport and cell performance. The baffles are arranged in the cathode flow channel in order to force the fuel gas to flow into the gas diffuser layer (GDL) and catalyst layer (CL). The baffles are located at the positions of $i/(iV+1)$th length from the cathode inlet as shown in Fig. 2. For example, for case of one baffle (i.e., $N=1$), the baffle location is on the location of the l/2 length from the inlet, that is, at the central position of the channel length. For $N=3$, the three baffles are located at the positions of 1/4, 1/2 and 3/4th length from the inlet, respectively. Consequently, to simplify the problem, a steady state, multi-species

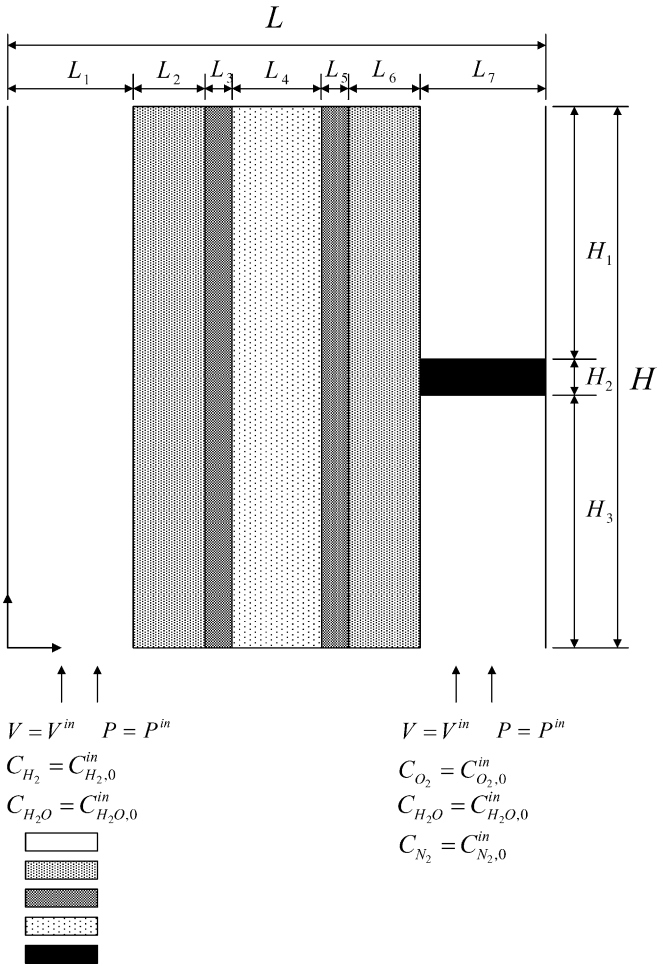

Fig. 1. Two-dimensional full cell model of a PEMFC system with baffle-blocked flow channel.

and along-the-channel model of a full cell PEMFC is employed for the analysis. Four species were considered: hydrogen, oxygen, nitrogen and water vapor. Stationary conditions are assumed in this fuel cell, also the effect of gravity is neglected. The GDL, CL and PEM are assumed to be isotropically porous materials. It is also assumed that the electrochemical reactions takes place only in the CL, and the gas mixtures in the flow channels are considered to be perfect gases. Based on the definition of the Reynolds number and the velocity used in this work, the flow in the fuel cell is laminar. Therefore, all the transport equations were formulated for laminar behavior.

According to the descriptions and assumption above, the basic transport equations for the two-dimensional PEM fuel cell are given as the following:

continuity equation:

$$\frac{\partial U}{\partial X} + \frac{\partial V}{\partial Y} = 0 \tag{1}$$

momentum equation:

$$U\frac{\partial U}{\partial X} + V\frac{\partial U}{\partial Y} = -\frac{1}{\rho}\frac{\partial P}{\partial X} + \nu\left(\frac{\partial^2 U}{\partial X^2} + \frac{\partial^2 U}{\partial Y^2}\right) + S_x \tag{2}$$

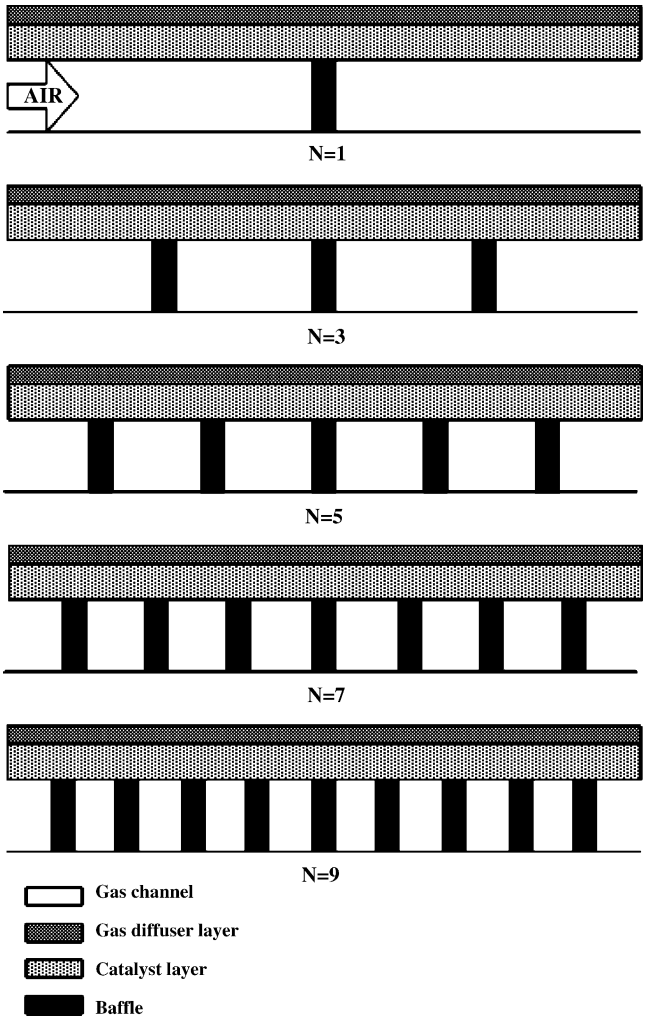

Fig. 2. Schematic of the half cell of PEM fuel cell with flow-blocked field design.

$$U\frac{\partial V}{\partial X}+V\frac{\partial V}{\partial Y}=-\frac{1}{\rho}\frac{\partial P}{\partial P}+\nu\left(\frac{\partial^2 V}{\partial X^2}+\frac{\partial^2 V}{\partial Y^2}\right)+S_y \tag{3}$$

species equation:

$$\varepsilon_{\text{eff}}\left(U\frac{\partial C_i}{\partial X}+V\frac{\partial C_i}{\partial Y}\right)=D_{i,\text{eff}}\left(\frac{\partial^2 C_i}{\partial X^2}+\frac{\partial^2 C_i}{\partial Y^2}\right)+S_{\text{c}}+S_{\text{L}} \tag{4}$$

and phase potential equation:

$$\frac{\partial}{\partial X}\left(\sigma_{\text{m}}\frac{\partial \Phi}{\partial X}\right)+\frac{\partial}{\partial Y}\left(\sigma_{\text{m}}\frac{\partial \Phi}{\partial Y}\right)=S_j \tag{5}$$

The S_x and S_y stand for the source terms based on the Darcy's drag forces in the X- and Y-directions imposed by the pore walls on the fluid, and usually cause in a significant pressure drop across the porous media. S_{c} is the production rates of ith species in gas phase, S_{L} represents the quality of liquid water and S_j is the source term for phase potential equation. The details of S_x, S_y, S_{c}, S_{L} and S_j for GDL, CL and PEM are listed in Table 1. In Table 1, the ε_{eff} is the effective porosity, C_{F} the quadratic drag factor, Z_{f} the charge transfer coefficient, C_{H^+} the concentration of proton, F the Faraday constant and k is the permeability using Blake–Kozeny correlation, Eq. (13), for modeling. In this correlation, $D_{\text{IP}}=6R_{\text{VS}}$, and R_{VS} is the volume-to-surface ratio of the porous material.

In the species equation, Eq. (4), the effective mass diffusivity, $D_{i,\text{eff}}$ is formulated by Bruggemann relation, Eq. (14). The parameters j_{a} and j_{c} indicate the current density at the anode and cathode sides, respectively, and can be described by the Butler–Volmer equations, Eq. (15), where Aj_0^{ref} is the exchange current density, α_{a} and α_{c} the electric charge transport rates in anode and cathode CLs, η the overpotential, R the gas constant and T is the temperature of the fuel cell.

In this work, the liquid water effect is taken into account by modifying the mass diffusivity due to the liquid water filling the pores in the porous media and the liquid water generation in the species concentration equation. When the partial pressure of water vapor is greater than the saturation pressure of water vapor, the water vapor is assumed to condense and fill the pore in the porous media. The source term, S_{L} in the species concentration equation, Eq. (9), representing the quality of liquid water can be formulated by Eq. (16), where M is the molecular weight and the k_{c} and k_{e} are the condensation and evaporation rate constants. The saturation pressure of water can be expressed as Eq. (17). In addition, the saturation, s, is defined as the ratio of the volume of pore occupied by liquid water to the volume of pore in the porous medium, then the effective porosity of porous media is modified to account the liquid water effect,

$$\varepsilon_{\text{eff}}=\varepsilon(1-s) \tag{19}$$

In the phase potential equation, σ_{m} is the electric conductivity of the membrane, which can be calculated by Eq. (18) developed by Springer et al. [2] and the reference electric conductivity is

$$\sigma_{\text{m}}^{\text{ref}}=0.005139\lambda-0.00326 \tag{20}$$

$$\lambda=\begin{cases}0.043+17.81a-39.85a^2+36.0a^3, & 0\le a\le 1\\ 14+1.4(a-1), & 1<a\le 3\end{cases} \tag{21}$$

In Eq. (21), a is the ability of water vapor at the cathode side. Using the following relations between the phase potential O and current density i,

$$i_x=-\sigma_{\text{m}}\frac{\partial \Phi}{\partial x} \tag{22}$$

$$i_y=-\sigma_{\text{m}}\frac{\partial \Phi}{\partial y} \tag{23}$$

Eq. (5) can then be reduced to be

$$\frac{\partial i_x}{\partial X}+\frac{\partial i_y}{\partial Y}=j_{\text{a}}\ \text{at anode} \tag{24}$$

$$\frac{\partial i_x}{\partial X}+\frac{\partial i_y}{\partial Y}=j_{\text{c}}\ \text{at cathode} \tag{25}$$

Boundary conditions for the dependent variables of the transport equations at the interfaces between different layers of the

Table 1
Equations used in the analysis

Equation	Expression		References
Source of x-momentum equation for GDL and CL	$S_x = -\frac{\nu\varepsilon_{\text{eff}}}{k}U - \frac{\varepsilon_{\text{eff}}^2 C_{\text{F}}\rho U}{\sqrt{k}}\sqrt{U^2+V^2}$	(6)	Wang and Cheng [21]; Wang et al. [22]
Source of y-momentum equation for GDL and CL	$S_y = -\frac{\nu\varepsilon_{\text{eff}}}{k}V - \frac{\varepsilon_{\text{eff}}^2 C_{\text{F}}\rho V}{\sqrt{k}}\sqrt{U^2+V^2}$	(7)	Wang and Cheng [21]; Wang et al. [22]
Source of x-momentum equation for PEM	$S_x = -\frac{\nu\varepsilon_{\text{eff}}}{k}U - \frac{\varepsilon_{\text{eff}}^2 C_{\text{F}}\rho U}{\sqrt{k}}\sqrt{U^2+V^2} + \frac{k}{\nu\varepsilon_{\text{eff}}}Z_{\text{f}}C_{\text{H}^+}F\nabla\Phi\frac{\partial U}{\partial X}$	(8)	Wang and Cheng [21]; Wang et al. [22]
Source of y-momentum equation for PEM	$S_y = -\frac{\nu\varepsilon_{\text{eff}}}{k}V - \frac{\varepsilon_{\text{eff}}^2 C_{\text{F}}\rho V}{\sqrt{k}}\sqrt{U^2+V^2} + \frac{k}{\nu\varepsilon_{\text{eff}}}Z_{\text{f}}C_{\text{E}^+}F\nabla\Phi\frac{\partial V}{\partial Y}$	(9)	Wang and Cheng [21]; Wang et al. [22]
Chemical source in species equation for hydrogen in CL	$S_{\text{c}} = \begin{cases} -\frac{j_{\text{a}}}{2FC_{\text{total,a}}} & \text{hydrogen} \\ -\frac{j_{\text{c}}}{4FC_{\text{total,c}}} & \text{oxygen} \\ -\frac{j_{\text{c}}}{2FC_{\text{total,c}}} & \text{water vapor} \end{cases}$	(10)	Gurau et al. [23]
Chemical source in species equation for proton in PEM	$S_{\text{c}} = \frac{ZF}{RT}D_{i,\text{eff},\text{H}^+}C_{\text{H}^+}\left(\frac{\partial^2\Phi}{\partial X^2}+\frac{\partial^2\Phi}{\partial Y^2}\right)$	(11)	Gurau et al. [23]
Source term for Phase potential	$S_j = \begin{cases} -j_{\text{a}} & \text{anode} \\ -0 & \text{membrane} \\ -j_{\text{c}} & \text{cathode} \end{cases}$	(12)	Gurau et al. [23]
Blake–Kozeny correlation	$k = \left(\frac{D_{\text{IP}}^2}{150}\right)\left[\frac{\varepsilon_{\text{eff}}^3}{(1-\varepsilon_{\text{eff}})^2}\right]$	(13)	Dullien [24]
Bruggemann relation	$D_{i,\text{eff}} = D_i\varepsilon_{\text{eff}}^{\tau}$; τ : tortuosity $= \begin{cases} 1.5 & \text{GDL, CL} \\ 6 & \text{PEM} \end{cases}$	(14)	Berning et al. [25]
Butler–Volmer expression	$j_{\text{a}} = Aj_0^{\text{ref}}\left(\frac{C_{\text{H}_2}}{C_{\text{H}_2}^{\text{ref}}}\right)\left[e^{(\alpha_{\text{a}}F/RT)\eta} - \frac{1}{e^{(\alpha_{\text{c}}F/RT)\eta}}\right]$; $j_{\text{c}} = Aj_0^{\text{ref}}\left(\frac{C_{\text{O}_2}}{C_{\text{O}_2}^{\text{ref}}}\right)\left[e^{(\alpha_{\text{a}}F/RT)\eta} - \frac{1}{e^{(\alpha_{\text{c}}F/RT)\eta}}\right]$	(15)	Gurau et al. [23]
Liquid water source in species equation	$S_{\text{L}} = \begin{cases} M_{\text{H}_2\text{O}}k_{\text{c}}\frac{\varepsilon_{\text{eff}}C_{\text{H}_2\text{O}}}{\rho RT}(P_{\text{H}_2\text{O}}-P_{\text{sat}}) & \text{if } P_{\text{H}_2\text{O}} > P_{\text{sat}} \\ k_{\text{e}}\varepsilon_{\text{eff}}s(P_{\text{sat}}-P_{\text{H}_2\text{O}}) & \text{if } P_{\text{H}_2\text{O}} > P_{\text{sat}} \\ k_{\text{e}}\varepsilon_{\text{eff}}s(P_{\text{sat}}-P_{\text{H}_2\text{O}}) & \text{if } P_{\text{H}_2\text{O}} > P_{\text{sat}} \end{cases}$	(16)	Mazumder and Cole [26]
Saturation pressure	$P_{\text{sat}} = 10^{-2.1794+0.02953T-9.1837\times10^{-5}T^2+1.4454\times10^{-7}T^3}$	(17)	Springer et al. [2]
Equation membrane conductivity	$\sigma_{\text{m}}(T) = \sigma_{\text{m}}^{\text{ref}}\exp\left[1268\left(\frac{1}{303}-\frac{1}{T}\right)\right]$	(18)	Springer et al. [2]

same domain are not required. At the gas channel outlet, the fully developed flow conditions are assumed,

$$U = \frac{\partial V}{\partial Y} = \frac{\partial C_i}{\partial Y} = 0 \tag{26}$$

The boundary conditions at the gas flow channel walls are

$$U = V = \frac{\partial C_i}{\partial X} = 0 \tag{27}$$

In practical situation, the physical properties and their gradients are continuous on the interface. So the natural boundary conditions on the interface are the same velocity, same concentration and the same gradients. At the interfaces between the GDLs and the gas channels, the following boundary conditions are used,

$$\varepsilon_{\text{eff},X^+}\left.\frac{\partial V}{\partial X}\right|_{X=X^+} = \left.\frac{\partial V}{\partial X}\right|_{X=X^-}, \quad V_{X=X^+} = V_{X=X^-} \tag{28}$$

$$\varepsilon_{\text{eff},X^+}\left.\frac{\partial C_i}{\partial X}\right|_{X=X_1^+} = \left.\frac{\partial C_i}{\partial X}\right|_{X=X_1^-}, \quad C_{i,X=X^+} = C_{i,X=X^-} \tag{29}$$

The similar conditions are employed for the interfaces between the GDLs and the CLs and the interfaces between the CLs and membrane can be expressed as follows:

$$\varepsilon_{\text{eff},X^+}\left.\frac{\partial V}{\partial X}\right|_{X=X^+} = \varepsilon_{\text{eff},X^-}\left.\frac{\partial V}{\partial X}\right|_{X=X^-}, \quad V_{X=X^+} = V_{X=X^-} \tag{30}$$

$$\varepsilon_{\text{eff},X^+}\left.\frac{\partial C_i}{\partial X}\right|_{X=X^+} = \varepsilon_{\text{eff},X^-}\left.\frac{\partial C_i}{\partial X}\right|_{X=X^-}, \quad C_{i,X=X^+} = V_{i,X=X^-} \tag{31}$$

The boundary conditions for the phase potential at the interface between the CL and the membrane are $\Phi = 0$ at the anode side, and $\frac{\partial \Phi}{\partial X} = 0$ at the cathode side. Because the phase potential is a linear distribution in the membrane, the phase potential boundary condition can be written as $\frac{\partial \Phi}{\partial Y} = 0$.

3. Numerical method

Since it is impossible to obtain an analytic solution of the complex convection–diffusion problem like this one, the solution to the governing equation will be solved by a finite volume method using a collocated cell-centred variable arrangement by dividing the model domain into a number of cells as control volumes. In the finite volume method, the governing equations are numerically integrated over each of these computational cells or control volumes. The governing equations can be expressed in the form of a generalized transport equation

$$\nabla(\rho\vec{u}\phi - \Gamma_\phi \nabla\phi) = S_\phi \tag{32}$$

where ϕ denotes the general dependent variable, Γ_ϕ the exchange coefficient, S_ϕ the source term, $\vec{u}$ the velocity vector and ρ is the density. With the discritization of the governing equations, the coupled finite-difference equations can be expressed in the form of

$$a_\text{p}\phi_\text{p} = a_\text{E}\phi_\text{E} + a_\text{W}\phi_\text{W} + a_\text{N}\phi_\text{N} + a_\text{s}\phi_\text{s} + S_\phi \tag{33}$$

where ϕ_p is the value of ϕ at the current point p, $\phi_\text{E} \ldots \phi_\text{s}$ stand for the values of the grid points adjacent to the point p, and $a_\text{p} \ldots a_\text{s}$ are known as the link coefficients.

In this work, the non-uniformly distributed grid systems of 103 and 77 points are employed in the x and y directions (or expressed as 103×77), respectively. To obtain better accuracy in the numerical computations, coarse and fine grid systems are considered in the preliminary tests. Effects of the grid number on the predictions of local current density are shown in Fig. 3. The maximum deviations among the computations on the grids of 73×57, 103×77 and 143×107 are less than 3%. Therefore, the grid system of 85×70 points seems to be sufficient to resolve the behaviors of the reactant gas transport in the present PEMFC model.

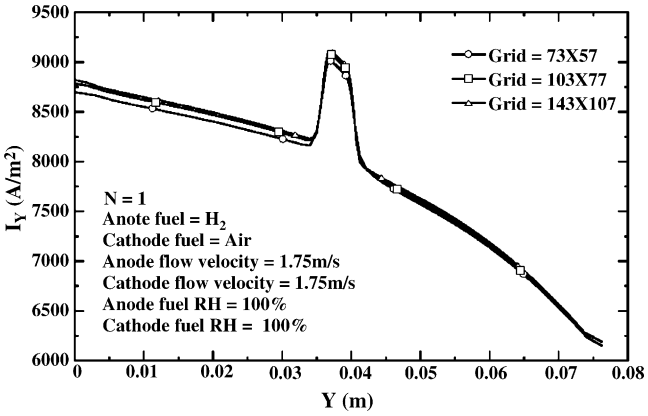

Fig. 3. Comparison of predictions on various grid systems.

4. Results and discussion

The total length of the flow channel is 7.62 cm, and the cross-section of the flow channel is 0.0762 cm × 0.0762 cm. The thicknesses of the GDL, CL and the membrane are fixed and set to be 0.0254, 0.00287 and 0.023 cm, respectively. The thickness of the baffle is taken as 0.3048 cm. The porosity is 0.4 for both GDL and CL. The inlet conditions for the PEM fuel cell are the inlet pressure with 101.3 kPa, inlet temperature with 353 K and inlet velocity with 1.75 m s^{-1} for both anode and cathode. In this analysis, the inlet relative humidities (RH) are chosen as 20%, 60% and 100% for both hydrogen and air in order to study the influence of inlet RH. Results without consideration of liquid water effect are also investigated.

The effect of RH of hydrogen gas on the cell performance is shown in Fig. 4. There are three baffles in the cathode for the analysis. It is seen that the cell performance of RH = 100% is the best of the three, and the cell performance decreases as the relative humidity decreases. This is because more water vapor helps the mass transfer of hydrogen, which in turns a better cell performance is obtained. Comparing results with and without consideration of liquid water effect, the cell performance with liquid water effect is lower than that without liquid water effect,

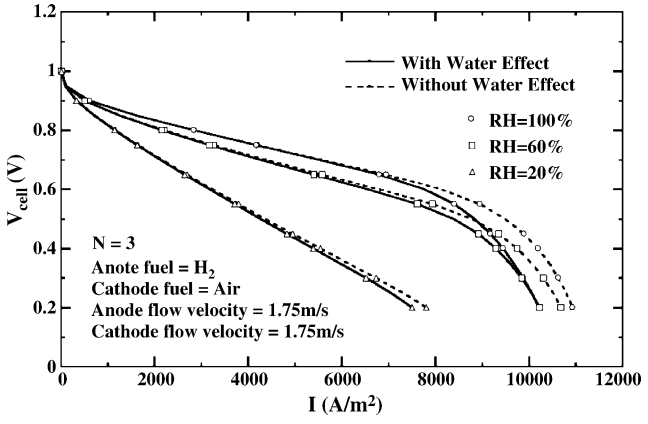

Fig. 4. Effects of relative humidity of hydrogen gas on anode side on the cell performance.

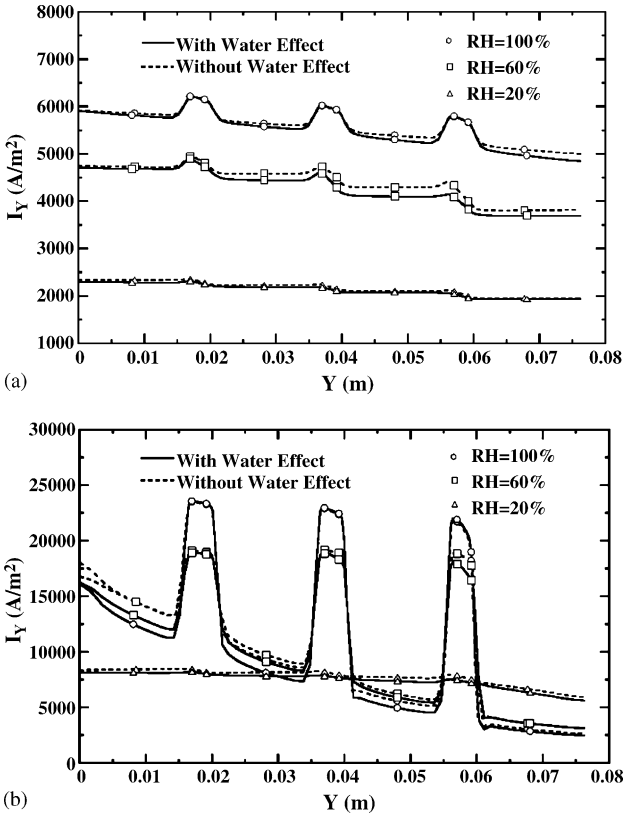

Fig. 5. Effects of relative humidity of hydrogen gas on anode side on the local current density distributions: (a) $V = 0.7$ V; (b) $V = 0.2$ V.

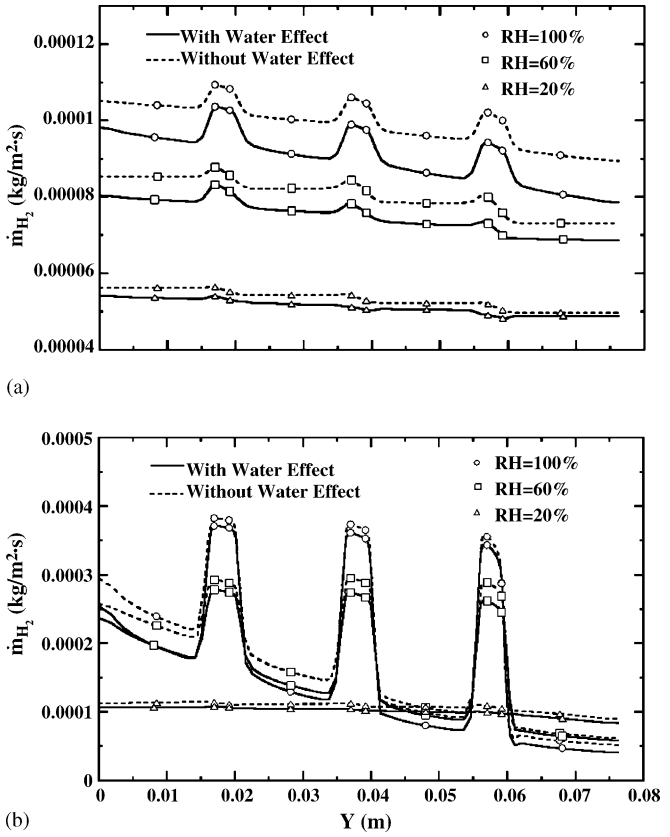

Fig. 6. Effects of relative humidity of hydrogen gas on anode side on the distributions of the hydrogen mass flow rate: (a) $V = 0.7$ V; (b) $V = 0.2$ V.

especially at lower voltage conditions. This indicates that more water is generated in the CL of the cathode and liquid water filled in the void of porous materials, causing the decrease in the cell performance. The two-phase flow should be considered at low voltage conditions.

The RH of hydrogen effects on the local current density distributions at $V = 0.7$ and 0.2 V are presented in Fig. 5. To investigate the liquid water effects, the results with and without considerations of liquid water in the modeling are both shown in Fig. 5. It is clearly seen that the local current density decreases along the axial direction, except for the baffle location with peak values. Due to the mass transport of hydrogen gas is increased through baffle-block mechanism, the local current density increases abruptly. It means that the cell performance is better around the baffle locations. However, the trend is not so obvious in the condition of RH = 20% for both 0.7 and 0.2 V. Apparently, this is due to the fact that the water content of the fuel streams is not enough to keep the membrane well hydrated thus resistance of the membrane and ohmic loses at the membrane are higher. An overall inspection on Fig. 5 indicates that the local current density increases as the RH increases. However, the local current density of RH = 60% at 0.2 V for $Y < 0.015$ m is larger than that of RH = 100%. The reason is that the back diffusion of liquid water prevents hydrogen gas from transport into diffusion layer resulted in a lower current density. It is also noticed that the local current density with RH = 60% is higher than that with RH = 100% between the baffles. This is due to the fact that the water removal by baffle-block effect accumulated between the baffles. It is found that the local current density with consideration of liquid water effect is always smaller than that without consideration of liquid water effect. However, the liquid water effect is not so obvious at the locations of baffles. This is due to the fact that the liquid water in the void of porous materials is removed by the shear force induced from the forced flow of the baffle.

The distributions of hydrogen mass flux along the interface between the GDL and CL in the anode of RH = 20%, 60% and 100% with $N = 3$ at $V = 0.7$ and 0.2 V are depicted in Fig. 6. It is clearly shown that the hydrogen mass flux decreases along the axial direction. This is due to the water accumulation in the void of the porous material, which in turn causes the reduction of chemical reaction and the mass transfer of hydrogen. It is also observed that the hydrogen mass flux increases as the inlet RH increases. This is because the water content in the fuel gas mixture is high, resulted in the reduction of the ohmic lost of membrane, which in turn increases the proton migration for the chemical reaction. This means that the consumption of hydrogen increases. It is interesting to see that the hydrogen mass flux increases abruptly at the locations of baffles in the cathode. This is because more oxygen mass flux in the cathode is forced into the gas diffusion layer at the baffle locations and more chemical reaction occurs resulting in more hydrogen mass consumption in the anode.

Fig. 7 shows the effect of humidity of hydrogen on the distribution of water mass flux at the GDL–CL interface of the

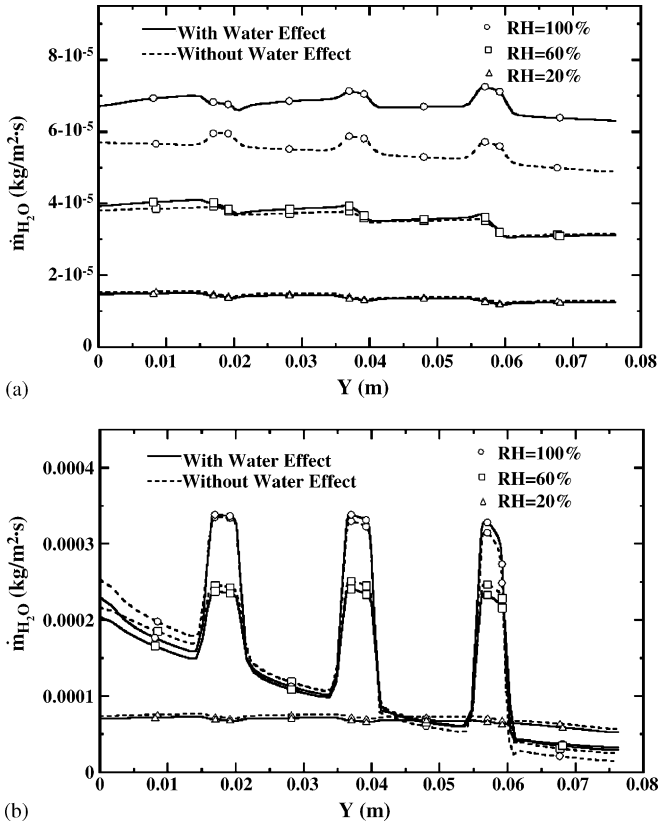

Fig. 7. Effects of relative humidity of hydrogen gas on anode side on the distributions of the mass flow rate of water vapor: (a) $V = 0.7$ V; (b) $V = 0.2$ V.

cathode with $N = 3$ at $V = 0.7$ and 0.2 V. It is found that the water mass flux increases as the inlet RH of hydrogen gas increases. This is due to water vapor in the hydrogen stream improves the mass transfer of hydrogen to the membrane, which leads to the increase of production of water at the GDL–CL interface of the cathode. It is also noticed that results without liquid water effect are underestimated compared with that with liquid water effect for RH = 60% and 100% at $V = 0.7$ V and the downstream region of $V = 0.2$ V. This is due to the fact that the chemical reaction is weak at high voltage conditions and the downstream region at low voltage conditions resulted in less water vapor produced than that in the fuel stream. This implies that the water mass flux is mainly from the water vapor in the fuel stream at high voltage conditions.

Since water is produced at the CL of the cathode in a PEM fuel cell, the mass transfer of air gas would be reduced due to liquid water condensation in the void of GDL of the cathode. Therefore, proper water management in the cathode would enhance the cell performance and preventing from flooding. In order to obtain a better understanding, the inlet RH of air gas in the cathode is also studied to investigate its influence on the cell performance, which is shown in Fig. 8. It is seen that the cell performance increases as the inlet RH decreases at low voltage conditions. This is due to the oxygen mass fraction of RH = 20% is the highest and more oxygen takes part in the chemical reactions, which in turn resulting in a better cell performance. However, it is not true for high voltage conditions. This is because the electro-

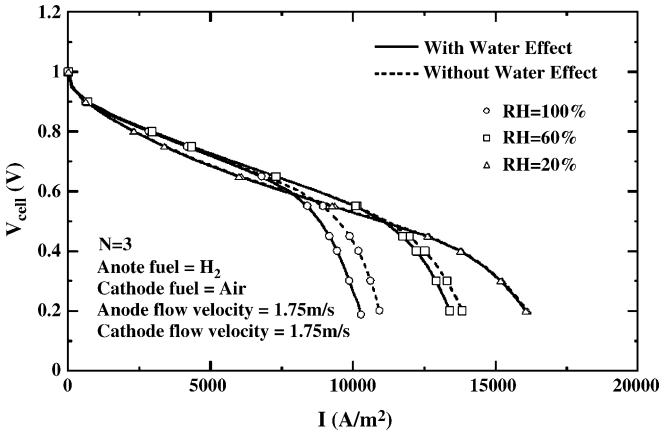

Fig. 8. Effects of relative humidity of air gas on cathode side on the cell performance.

chemical reaction is weak and the water effect is not obvious. As the operating voltage decreases, the chemical reaction becomes stronger and more water is produced. The influence of liquid water becomes more important and the effect of liquid water should be taken into account on the cell performance. Fig. 9 presents the influence of inlet RH of air gas in the cathode side on the distribution of local current density. It is found that the local current density of RH = 20% is the lowest of the three at high voltage conditions, while the highest at low voltage conditions. Because the chemical reaction is weak at high voltage

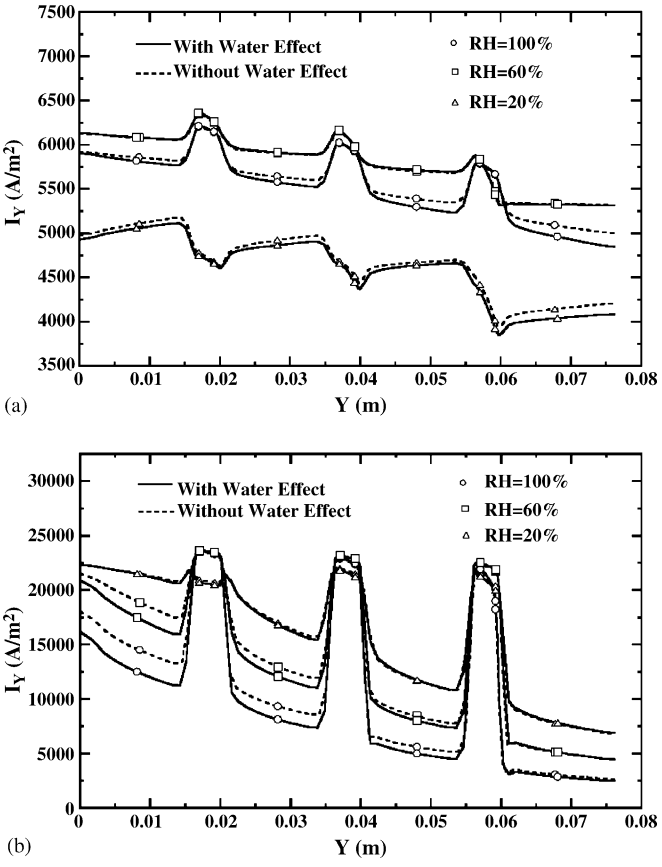

Fig. 9. Effects of relative humidity of air gas on cathode side on the distributions of the local current density: (a) $V = 0.7$ V; (b) $V = 0.2$ V.

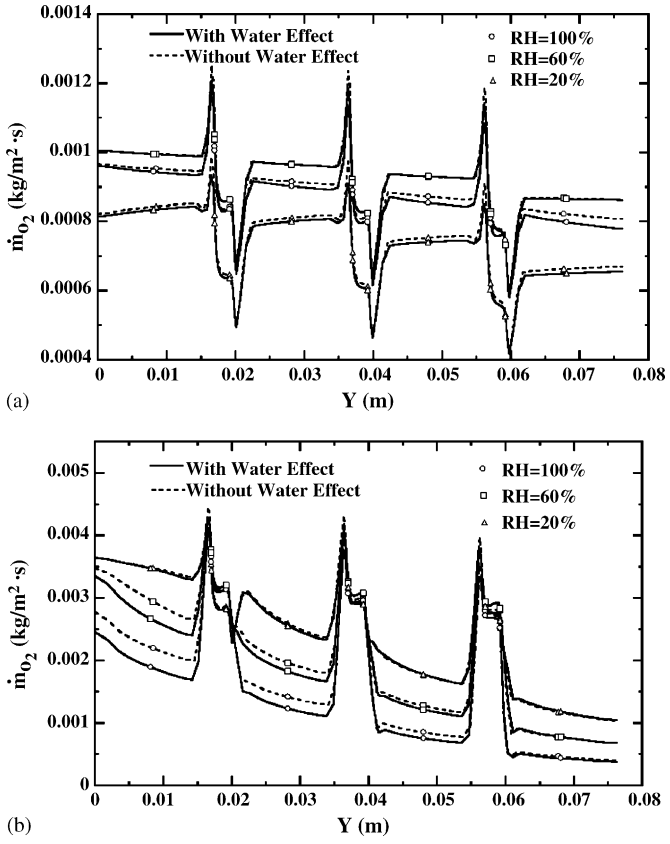

Fig. 10. Effects of relative humidity of air gas on cathode side on the distributions of oxygen mass flow rate: (a) $V = 0.7$ V; (b) $V = 0.2$ V.

conditions, the liquid water effect is not so obvious. However, at low voltage conditions, the chemical reactions become stronger resulted in the reduction of oxygen mass transfer due to liquid water produced in the cathode.

Since the power output is the consequence of the electrochemical reaction, the consumption of the oxygen along the GDL–CL interface can be considered as an index of the cell performance. The effect of RH of air gas on cathode side on the distributions of oxygen mass flow rate along the interface between the GDL and CL with $N = 3$ are presented in Fig. 10. Around the baffle regions, the oxygen distributions show a peaked increase, which is a consequence of the channel blockage. Therefore, the oxygen distributions show peak variations around the baffles. It is observed that the oxygen mass flux of RH = 60% is the highest at high voltage conditions, while that of RH = 20% is the highest at low voltage conditions. This is due to the liquid water occupies the void of in the porous material leading the reduction of oxygen mass flux at high voltage conditions. It is also depicted that the distribution of oxygen mass flux presents an unordinary profile at the baffle locations. At the entrance of the flow channel, oxygen diffuses into the GDL and CL. Then oxygen mass flux is enhanced by the forced convection induced by the blockage of the baffles in the cathode. However, the remaining oxygen which is not involved in the chemical reaction diffuses back to the flow channel resulted in the reduction of oxygen mass flux. This is not found in low voltage conditions because the chemical reaction is much stronger at low voltage conditions.

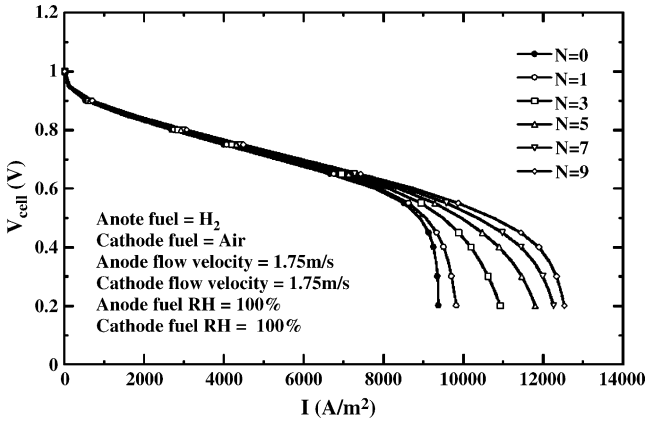

Fig. 11. Effects of baffle number on the cell performance.

Figs. 11 and 12 present the effects of baffle number on the cell performance and local current density distributions, respectively. It is obvious from Fig. 11 that the cell performance increases as N increases, especially at low voltage conditions. With the tandem arrangement of the baffles in the channel of the cathode side, the fuel gas is forced to flow into the GDL and CL to enhance the chance of chemical reaction at the CL as well as the performance of the fuel cell system.

The increase in N resulted in more oxygen transport into GDL and more chemical reaction occurs, which in turn increases the cell performance. However, it should be noted that the extent

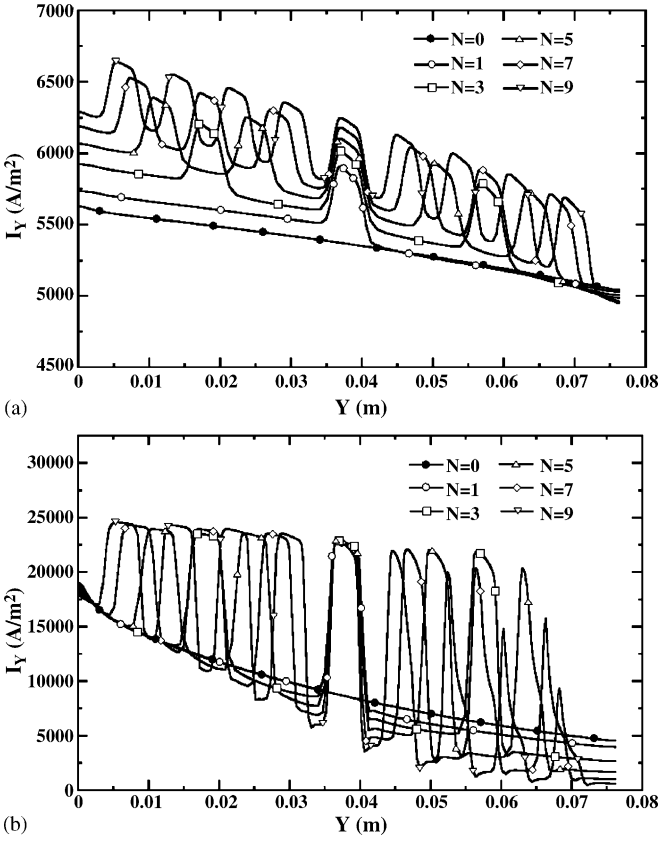

Fig. 12. Effects of baffle number on the local current density distributions: (a) $F = 0.7$ V; (b) $F = 0.2$ V.

of increase in the current density at low voltages decreases as N is larger than 3. This implies that there exists a limitation of the baffle number beyond that the cell performance would not increase significantly. That is, there is an optimal N. Fig. 12 shows local current density distributions of a periodic pattern with peak-value appearing in the regions around the baffles and reducing along the channel. With a careful inspection on Fig. 12, it is noted that the peak local current density increases as N increases at high voltage conditions, while that at a lower operating voltage remains about the same value. However, the peak current density at lower operating voltages for $N = 5$, 7 and 9 decreases at the downstream of the flow channels. This is due to the fact that the increase of number of baffles increases the fuel consumption resulting in the reacting fuel decreases at the downstream of the flow channels, which in turn causing the decrease in the local current density. The dramatic degradation in local current density in the downstream region of a blocked channel is a reflection of the more efficient fuel transport and the chemical reaction in the upstream.

5. Concluding remarks

A two-dimensional numerical model of PEMFC with baffle-blocked in cathode flow channel design is established to examine the effects of humidity of reactant gases at the inlet on the gas transport and cell performance of the PEM fuel cell. The effects of inlet relative humidity of reactant gases on both anode and cathode sides on the cell performance are considered. The effect of baffle numbers on the detailed transport phenomena of the PEM fuel cell with baffle-blocked flow field is also examined in detail. Brief summaries are as the following:

1. As the inlet relative humidity of hydrogen gas increases, both the chemical reaction and mass transfer of hydrogen are enhanced due to the increase of water content in the membrane, which leads to a better cell performance.
2. The increases of inlet relative humidity in the cathode side at lower operating voltages leads to the reduction of oxygen concentration. Therefore, the cell performance decreases with higher RHs. However, a better cell performance with lower RH at higher operating conditions is obtained due to more liquid water produced and filled the pore in the porous material reduces the mass transfer of oxygen.
3. It is discovered that the liquid water effect is less at high operating voltage conditions, because the chemical reaction is weak at high operating voltage resulting less water is produced. This indicates that the liquid water effect can be ignored at high operating voltage conditions.
4. The cell performance is increased as N increases. This implies that the area of forced convection is enlarged and more oxygen gas is forced into the catalyst layer. Therefore, the chemical reaction is enhanced resulted in the rise of cell performance. However, the amount of increase in the current density at low voltages decreases as the increase of number of baffles. That is, there is an optimum number of baffles that increases the cell performance.

Acknowledgements

The study was supported by the National Science Council, the Republic of China, through the grant numbers NSC 92-2218-E-211-001. And the financial support from the Northern Taiwan Institute of Science and Technology is also appreciated.

References

[1] D.M. Bernadi, M.W. Verbruge, AIChE J. 37 (8) (1991) 1151–1163.
[2] T.E. Springer, T.A. Zawodzinski, S. Gottesfeld, J. Electrochem. Soc. 138 (8) (1991) 2334–2341.
[3] T.F. Fuller, J. Newman, J. Electrochem. Soc. 140 (5) (1993) 1218–1225.
[4] T.V. Nguyen, R.E. White, J. Electrochem. Soc. 140 (8) (1993) 2178–2186.
[5] M. Cappadonia, J.W. Erning, S.M.S. Niaki, U. Stimming, Solid State Ionics 77 (1995) 65.
[6] T.A. Zawodziniski, T.E. Springer, F. Uribe, S. Gottesfeld, Solid State Ionics 60 (1993) 199.
[7] S. Yoshioka, A. Yoshimura, H. Fukumoto, O. Hiroi, H. Yoshiyasu, J. Power Sources 144 (2005) 146–151.
[8] N. Rajalakshmi, P. Sridhar, K.S. Dhathathreyan, J. Power Sources 109 (2002) 452–457.
[9] D. Hyun, J. Kim, J. Power Sources 126 (2004) 98–103.
[10] I.S. Yi, T.V. Nguyen, J. Electrochem. Soc. 145 (4) (1998) 1149–1159.
[11] S.H. Ge, B.L. Yi, J. Power Sources 124 (2003) 1–11.
[12] J.J. Baschuk, X. Li, J. Power Sources 86 (2000) 181–196.
[13] I.M. Hsing, P. Futerko, Chem. Eng. Sci. 55 (2000) 4209–4218.
[14] T.V. Nguyen, J. Electrochem. Soc. 143 (5) (1996) 103–105.
[15] S. Um, C.Y. Wang, The 2000 ASME International Mechanical Engineering Congress & Exposition, November 5–10, 2000, Walt Disney World Dolphin, Orlando, FL, USA, 2000.
[16] S. Um, C.Y. Wang, K.S. Chen, J. Electrochem. Soc. 147 (2000) 4485–4493.
[17] W. He, J.S. Yi, T.V. Nguyen, AIChE J. 46 (10) (2000) 2053–2064.
[18] A. Kazim, H.T. Liu, P. Forges, J. Appl. Electrochem. 29 (1999) 1409–1416.
[19] W.M. Yan, C.Y. Soong, F. Chen, H.S. Chu, J. Power Sources 125 (2004) 27–39.
[20] H.C. Liu, W.M. Yan, C.Y. Soong, F. Chen, J. Power Sources 142 (2005) 125–133.
[21] C.Y. Wang, P. Cheng, Adv. Heat Transfer 30 (1997) 93.
[22] C.Y. Wang, W.B. Gu, B.Y. Liaw, J. Electrochem. Soc. 145 (1998) 3047–3057.
[23] V. Gurau, H. Liu, S. Kakac, AIChE J. 44 (1998) 2410–2422.
[24] F.A.L. Dullien, Porous Media, Academic Press, New York, 1991.
[25] T. Berning, D.M. Lu, N. Djilali, J. Power Sources 106 (2002) 284–294.
[26] S. Mazumder, J.V. Cole, J. Electrochem. Soc. 150 (2003) 1510–1517.